Mapping the Antigenic and Genetic Evolution of Influenza Virus

Derek J. Smith *et al.*

Science **305**, 371 (2004);
DOI: 10.1126/science.1097211

Science (print ISSN 0036-8075; online ISSN 1095-9203) is published weekly, except the last week in December, by the American Association for the Advancement of Science, 1200 New York Avenue NW, Washington, DC 20005.

CO_2 from preindustrial levels will result in a 30% decrease in carbonate ion concentration and a 60% increase in hydrogen ion concentration. As the carbonate ion concentration decreases, the Revelle factor increases and the ocean's ability to absorb more CO_2 from the atmosphere is diminished. The impact of this acidification can already be observed today and could have ramifications for the biological feedbacks in the future (*26*). If indeed the net feedbacks are primarily positive, the required socioeconomic strategies to stabilize CO_2 in the future will be much more stringent than in the absence of such feedbacks. Future studies of the carbon system in the oceans should be designed to identify and quantitatively assess these feedback mechanisms to provide input to models that will determine the ocean's future role as a sink for anthropogenic CO_2.

References and Notes

1. P. J. Crutzen, E. F. Stoermer, *Global Change Newslett.* **41**, 12 (2000).
2. R. A. Houghton, J. L. Hackler, in *Trends: A Compendium of Data on Global Change* (Carbon Dioxide Information Analysis Center, Oak Ridge National Laboratory, TN, 2002), http://cdiac.esd.ornl.gov/trends/landuse/houghton/houghton.html.
3. C. Prentice *et al.*, in *Climate Change 2001: The Scientific Basis. Contribution of Working Group I to the Third Assessment Report of the Intergovernmental Panel on Climate Change*, J. T. Houghton *et al.*, Eds. (Cambridge Univ. Press, New York, 2001), pp. 183–237.
4. D. W. R. Wallace, in *Ocean Circulation and Climate*, G. Siedler, J. Church, W. J. Gould, Eds. (Academic Press, San Diego, CA, 2001), pp. 489–521.
5. R. M. Key *et al.*, in preparation.
6. Bottle data and 1° gridded distributions are available through the GLODAP Web site (http://cdiac.esd.ornl.gov/oceans/glodap/Glodap_home.htm).
7. N. Gruber, J. L. Sarmiento, T. F. Stocker, *Global Biogeochem. Cycles* **10**, 809 (1996).
8. C. L. Sabine *et al.*, *Global Biogeochem. Cycles* **13**, 179 (1999).
9. C. L. Sabine *et al.*, *Global Biogeochem. Cycles* **16**, 1083, 10.1029/2001GB001639 (2002).
10. K. Lee *et al.*, *Global Biogeochem. Cycles* **17**, 1116, 10.1029/2003GB002067 (2003).
11. Materials and methods are available as supporting material on *Science* Online.
12. R. Revelle, H. E. Suess *Tellus* **9**, 18 (1957).
13. T. Takahashi, J. Olafsson, J. G. Goddard, D. W. Chipman, S. C. Sutherland, *Global Biogeochem. Cycles* **7**, 843 (1993).
14. Five intermediate water masses and NADW were defined using the following temperature (T) and salinity (S) properties: Pacific AAIW: $33.8 < S < 34.5$ and $2 < T < 10$; NPIW: $S < 34.3$ and $5 < T < 12$; Indian AAIW: $33.8 < S < 34.5$ and $2 < T < 10$; Red Sea Water: $S > 34.8$ and $5 < T < 14$; Atlantic AAIW: $33.8 < S < 34.8$ and $2 < T < 6$; NADW: $34.8 < S < 35$ and $1.5 < T < 4$. Water mass inventories were determined by summing up the gridded anthropogenic CO_2 values within a region defined by the T and S limits using the Levitus World Ocean Atlas 2001 salinity and temperature fields.
15. A. Papaud, A. Poisson, *J. Mar. Res.* **44**, 385 (1986).
16. S. Mecking, M. Warner, *J. Geophys. Res.* **104**, 11087 (1999).
17. A. Poisson, C.-T. A. Chen, *Deep-Sea Res. Part A* **34**, 1255 (1987).
18. M. Stuiver, P. D. Quay, H. G. Ostlund, *Science* **219**, 849 (1983).
19. G. Marland, T. A. Boden, R. J. Andres, in *Trends: A Compendium of Data on Global Change* (Carbon Dioxide Information Analysis Center, Oak Ridge National Laboratory, TN, 2003), http://cdiac.esd.ornl.gov/trends/emis/meth_reg.htm.
20. D. M. Etheridge *et al.*, *J. Geophys. Res.* **101**, 4115 (1996).
21. C. D. Keeling, T. P. Whorf, in *Trends: A Compendium of Data on Global Change* (Carbon Dioxide Information Analysis Center, Oak Ridge National Laboratory, TN, 2004), http://cdiac.esd.ornl.gov/trends/co2/sio-keel.htm.
22. R. S. de Fries, C. B. Field, I. Fung, G. J. Collatz, L. Bounoua, *Global Biogeochem. Cycles* **13**, 803 (1999).
23. C. L. Sabine *et al.*, in *The Global Carbon Cycle: Integrating Humans, Climate, and the Natural World. SCOPE 62*, C. B. Field, M. R. Raupach, Eds. (Island Press, Washington, DC, 2004), pp. 17–44.
24. D. E. Archer, H. Kheshgi, E. Maier-Reimer, *Global Biogeochem. Cycles* **12**, 259 (1998).
25. N. Gruber *et al.*, in *The Global Carbon Cycle: Integrating Humans, Climate, and the Natural World. SCOPE 62*, C. B. Field, M. R. Raupach, Eds. (Island Press, Washington, DC, 2004), pp. 45–76.
26. R. A. Feely *et al.*, *Science* **305**, 362 (2004).

27. We thank all individuals who contributed to the global data set compiled for this project, including those responsible for the hydrographic, nutrient, oxygen, carbon, and chlorofluorocarbon measurements, and the chief scientists. The amount of work that went into collecting, finalizing, and synthesizing these data in a manner that makes a publication like this possible can never be properly acknowledged. This work was funded by grants from NOAA/U.S. Department of Energy and NSF. Partial support for K.L. was also provided by the Advanced Environmental Biotechnology Research Center at Pohang University of Science and Technology. This is Pacific Marine Environmental Laboratory contribution number 2683.

Supporting Online Material

www.sciencemag.org/cgi/content/full/305/5682/367/DC1
Materials and Methods
Fig. S1
Table S1

2 March 2004; accepted 8 June 2004

Mapping the Antigenic and Genetic Evolution of Influenza Virus

Derek J. Smith,[1,2]*† Alan S. Lapedes,[3]* Jan C. de Jong,[2] Theo M. Bestebroer,[2] Guus F. Rimmelzwaan,[2] Albert D. M. E. Osterhaus,[2] Ron A. M. Fouchier[2]*

The antigenic evolution of influenza A (H3N2) virus was quantified and visualized from its introduction into humans in 1968 to 2003. Although there was remarkable correspondence between antigenic and genetic evolution, significant differences were observed: Antigenic evolution was more punctuated than genetic evolution, and genetic change sometimes had a disproportionately large antigenic effect. The method readily allows monitoring of antigenic differences among vaccine and circulating strains and thus estimation of the effects of vaccination. Further, this approach offers a route to predicting the relative success of emerging strains, which could be achieved by quantifying the combined effects of population level immune escape and viral fitness on strain evolution.

Much of the burden of infectious disease today is caused by antigenically variable pathogens that can escape from immunity induced by prior infection or vaccination. The degree to which immunity induced by one strain is effective against another is mostly dependent on the antigenic difference between the strains; thus, the analysis of antigenic differences is critical for surveillance and vaccine strain selection. These differences are measured in the laboratory in various binding assays (*1*–*3*). Such assays give an approximation of antigenic differences, but are generally considered unsuitable for quantitative analyses. We present a method, based on the fundamental ideas described by Lapedes and Farber (*4*), that enables a reliable quantitative interpretation of binding assay data, increases the resolution at which antigenic differences can be determined, and facilitates visualization and interpretation of antigenic data. We used this method to study quantitatively the antigenic evolution of influenza A (H3N2) virus, revealing both similarities to, and important differences from, its genetic evolution.

Influenza viruses are classic examples of antigenically variable pathogens and have a seemingly endless capacity to evade the immune response. Influenza epidemics in humans cause an estimated 500,000 deaths worldwide per year (*5*). Antibodies against the viral surface glycoprotein hemagglutinin (HA) provide protective immunity to influenza virus infection, and this protein is therefore the primary component of influenza vaccines. However, the antigenic structure of HA has changed significantly over time, a process known as antigenic drift (*6*), and in most years, the influenza vaccine has to be up-

[1]Department of Zoology, University of Cambridge, Downing Street, Cambridge CB2 3EJ, UK. [2]National Influenza Center and Department of Virology, Erasmus Medical Center, Dr. Molewaterplein 50, 3015GE Rotterdam, Netherlands. [3]Theoretical Division, T-13, MS B213, Los Alamos National Laboratory, Los Alamos, NM 87545, USA.

*These authors contributed equally to this work.
†To whom correspondence should be addressed. E-mail: dsmith@zoo.cam.ac.uk

dated to ensure sufficient efficacy against newly emerging variants (*7*, *8*). The World Health Organization coordinates a global influenza surveillance network, currently consisting of 112 national influenza centers and four collaborating centers for reference and research. This network routinely characterizes the antigenic properties of influenza viruses using a hemagglutination inhibition (HI) assay (*1*). The HI assay is a binding assay based on the ability of influenza viruses to agglutinate red blood cells and the ability of animal antisera raised against the same or related strains to block this agglutination (*9*). Additional surveillance information is provided by sequencing the immunogenic HA1 domain of the HA gene for a subset of these strains. The combined antigenic, epidemiological, and genetic data are used to select strains for use in the vaccine.

Retrospective quantitative analyses of the genetic data have revealed important insights into the evolution of influenza viruses (*10*–*13*). However, the antigenic data are largely unexplored quantitatively because of difficulties in interpretation, even though antigenicity is a primary criterion for vaccine strain selection and is thought to be the main driving force of influenza virus evolution. When antigenic data have been analyzed quantitatively, it has usually been with the methods of, or methods equivalent to, numerical taxonomy (*14*–*16*). These methods have provided insights (*15*–*19*); however, they sometimes give inconsistent results, do not properly interpret data that are below the sensitivity threshold of the assay, and approximate antigenic distances between strains in an indirect way [discussed by (*4*, *16*, *18*)]. Lapedes and Farber (*4*) solved these problems with a geometric interpretation of binding assay data, in which each antigen and antiserum is assigned a point in an "antigenic map" [based on the theoretical concept of "shape space" (*20*–*23*)], such that the distance between an antigen and antiserum in the map directly corresponds to the HI measurement. Lapedes and Farber used ordinal multidimensional scaling (MDS) (*24*) to position the antigens and antisera in the map.

The method used in this manuscript is based on the fundamental ideas described by Lapedes and Farber (*4*) and, in particular, takes advantage of their observation that antigenic distance is linearly related to the logarithm of the HI measurement. Exploiting this observation allowed us to create a new method that is parametric yet still handles HI measurements that are beyond the sensitivity of the HI assay (*9*). We use a modification of metric MDS (*25*) to position the antigens and antisera in the map (*9*). This new approach offers computational advantages over the ordinal approach, including reduced running time and fewer local minima, making it tractable to run on datasets the size of the one used in this manuscript, and on larger datasets.

Antigenic map of human influenza A (H3N2) virus. We applied this method to mapping the antigenic evolution of human influenza A (H3N2) viruses, which became widespread in humans during the 1968 Hong Kong influenza pandemic and have been a major cause of influenza epidemics ever since. Antigenic data from 35 years of influenza surveillance between 1968 and 2003 were combined into a single dataset. We sequenced the HA1 domain of a subset of these virus isolates (*26*, *27*) and restricted the antigenic analysis to these sequenced isolates to facilitate a direct comparison of antigenic and genetic evolution. The resulting antigenic dataset consisted of a table of 79 postinfection ferret antisera by 273 viral isolates, with 4215 individual HI measurements as entries in the table. Ninety-four of the isolates were from epidemics in the Netherlands, and 179 were from elsewhere in the world.

We constructed an antigenic map from this dataset to determine the antigenic evolution of influenza A (H3N2) virus from 1968 to 2003 (Fig. 1). Because antigen-antiserum distances in the map correspond to HI values, it was possible to predict HI values that were missing in the original dataset and subsequently to measure those values using the HI assay, so as to determine the resolution of the map. We predicted and then measured 481 such HI values with an average absolute prediction error of 0.83 (SD 0.67) units (each unit of antigenic distance corresponds to a twofold dilution of antiserum in the HI assay) and a correlation between predicted and measured values of 0.80 ($p << 0.01$). The accuracy of these predictions indicates that the map has resolution higher than that previously considered available from HI data and higher than the resolution of the assay. The resolution of the map can be greater than the resolution of the assay because the location of a point in the map is fixed by measurements to multiple other points, thereby averaging out errors (*9*).

The map reveals high-level features of the antigenic evolution of influenza A (H3N2) virus. The strains tend to group in clusters rather than to form a continuous antigenic lineage, and the order of clusters in the map is mostly chronological; from the original Hong Kong 1968 (HK68) cluster, to the most recent Fujian 2002 (FU02) cluster. The antigenic distance from the HK68 cluster, through consecutive cluster centers, to the FU02 cluster is 44.6 units, and the average antigenic distance between the centers of consecutive clusters is 4.5 (SD 1.3) units. The influenza vaccine is updated between influenza seasons when there is an antigenic difference of at least 2 units between the vaccine strain and the strains expected to circulate in the next season; thus, not unexpectedly, we find at least one vaccine strain in each cluster.

The ability to define antigenic clusters allows us to identify the amino acid substitutions that characterize the difference between clusters (Table 1, fig. S1). Some of these "cluster-difference" substitutions (*9*) will contribute to the antigenic difference between clusters, some may be compensatory muta-

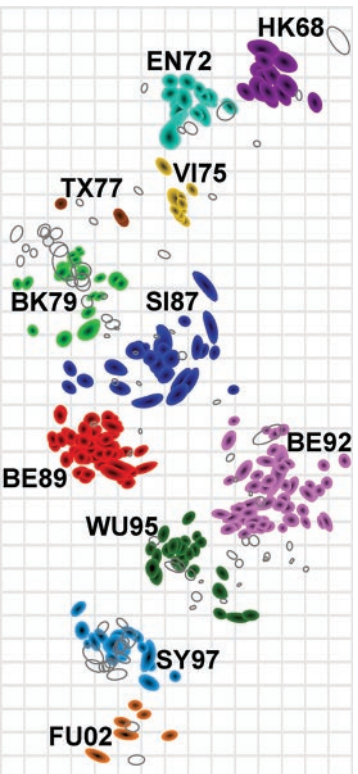

Fig. 1. Antigenic map of influenza A (H3N2) virus from 1968 to 2003. The relative positions of strains (colored shapes) and antisera (uncolored open shapes) were adjusted such that the distances between strains and antisera in the map represent the corresponding HI measurements with the least error (*9*). The periphery of each shape denotes a 0.5-unit increase in the total error; thus, size and shape represent a confidence area in the placement of the strain or antiserum. Strain color represents the antigenic cluster to which the strain belongs. Clusters were identified by a *k*-means clustering algorithm (*9*) and named after the first vaccine-strain in the cluster—two letters refer to the location of isolation (Hong Kong, England, Victoria, Texas, Bangkok, Sichuan, Beijing, Wuhan, Sydney, and Fujian) and two digits refer to year of isolation. The vertical and horizontal axes both represent antigenic distance, and, because only the relative positions of antigens and antisera can be determined, the orientation of the map within these axes is free. The spacing between grid lines is 1 unit of antigenic distance—corresponding to a twofold dilution of antiserum in the HI assay. Two units correspond to fourfold dilution, three units to eightfold dilution, and so on.

tions to retain function, and others may be hitchhikers carried along by chance. Of the 67 cluster-difference amino acid substitutions, 63 were in antigenic sites (*28*), 8 were in the receptor-binding site (*29*), and 21 were in codons previously identified as positively selected in an independent genetic dataset covering 1985 to 1997 (*10*). We see two patterns with respect to these positively selected codons: For the cluster transitions that happened during the period from 1985 to 1997—the period of the sample used to calculate the positively selected codons—most (10 of 12) of the cluster-difference substitutions were in positively selected codons; whereas outside of this timeframe, most [44 of 55, or 16 of 20 if the underrepresented Texas 1977 (TX77) and FU02 clusters are excluded] were not in positively selected codons. A possible explanation for this difference is that cluster-difference substitutions are positively selected, but that the positively selected codons have changed over time, resulting in some pre-1985 positively selected codons not being previously identified, possibly because they were underrepresented in the dataset used by Bush *et al*. (*10*). Other possible explanations are that not all cluster-difference substitutions are positively selected or that they cannot be detected as such with methods that use only genetic information.

Comparison of antigenic and genetic evolution. To further investigate the genetic basis of the antigenic cluster structure, we generated a maximum likelihood (ML) phylogenetic tree and a "genetic map" of the HA1 sequences of strains used in the antigenic analysis and color-coded both according to the clusters identified in the antigenic map of Fig. 1 (Fig. 2). The genetic map facilitates a side-by-side comparison with the antigenic map and is a visualization of the amino acid distance matrix calculated from the alignment of HA1 sequences (*9*). Previous comparisons of the antigenic and genetic evolution have revealed important insights (*6*, *19*, *30, 31*); however, a quantitative comparison has not been possible until now because of the previously low resolution of the antigenic data.

We find a remarkable overall correspondence between the relative positions of clusters in the genetic and antigenic maps (Fig. 2, B and C, respectively). The correlation between antigenic distance and the number of amino acid substitutions between strains was 0.81, and on average, 2.9 amino acid substitutions resulted in one unit change in antigenic distance. The rate of antigenic evolution per amino acid substitution was slower within clusters [on average 3.1 (SD 0.06) amino acid substitutions for each unit of antigenic change] than between clusters [on average 2.1 (SD 0.17) amino acid substitutions for each unit of antigenic change].

There is also a correspondence between the phylogenetic tree and antigenic map, with closely related nucleotide sequences generally belonging to the same antigenic cluster (Fig. 2, A and C). The correlation between antigenic distance and ML phylogenetic tree distance between strains was 0.78, and on average, an ML distance of 0.0085 corresponded to a 1-unit change in antigenic distance.

Although antigenic clusters are mostly contiguous when shown on the phylogenetic tree and genetic map (Fig. 2, A and B), it is not possible to reliably determine antigenic clusters from these genetic data alone. From the tree, it

Table 1. Cluster-difference amino acid substitutions, and distances between antigenic clusters. Cluster-difference amino acid substitutions defined in (*9*), antibody binding sites defined by (*28*). Substitution *at a codon in the receptor binding site (*29*); †at a codon with a rapid rate of amino acid replacement but not positively selected (*11*); and ‡at a positively selected codon (*10*). The TX77 and FU02 clusters are represented by fewer strains than other clusters; thus, the number of cluster-difference substitutions into and out of these clusters might decrease with more strains in these clusters. Cluster transitions follow the chronological order of cluster dominance, which is occasionally different from the genetic lineage. Antigenic and genetic distances are between cluster centroids in the antigenic map (Fig. 1) and genetic map (Fig. 2B), respectively. The average standard error (SE) for the genetic distances between clusters was 0.9, for the antigenic distances between clusters was 0.3, and for the ratio was 0.3 (table S1).

Cluster transition	Genetic distance (aa changes)	Antigenic distance (units)	Genetic antigenic ratio	Cluster-difference substitutions					
				Site A	Site B	Site C	Site D	Site E	Other
HK68-EN72	12.1	3.4	3.6	T122N G144D	T155Y* N188D		R207K		
EN72-VI75	14.6	4.4	3.3	N137S*† S145N‡	L164Q Q189K S193D‡	N53D I278S	F174S R102K‡ I213V I217V I230V		
V175-TX77	14.8	3.4	4.4	S137Y*†	G158E‡ Q164L D193N‡	K50R† D53N	S174F K201R‡ V213I V230I	E82K M260I	
TX77-BA79	16.0	3.3	4.8	N133S‡ P143S G146S	K156E‡ T160K Q197R‡	N53D N54S	D172G† V217I V244L	162K K82E	
BA79-SI87	11.9	4.9	2.4	G124D‡	Y155H* K189R				
SI87-BE89	6.9	4.6	1.5	N145K‡					
BE89-BE92	13.7	7.8	1.8	S133D‡ K145N‡	E156K‡ E190D*‡			T262N‡	
BE92-WU95	9.9	4.6	2.2	N145K‡					
WU95-SY97	16.0	4.7	3.4		K156Q‡ E158K‡ V196A†	N276K†		K62E	
SY97-FU02	16.0	3.5	4.5	A131T	H155T* Q156H‡	R50G†		H75Q E83K	L25I V202I W222R G225D*
Total	131.9	44.6							
Average	13.2	4.5	3.2						
SD	2.9	1.3	1.1						

is rarely obvious if a branch or lineage belongs to the same or a different antigenic cluster as its neighbors, and from the genetic map, it is not always possible to determine where one antigenic cluster ends and another begins. The most striking example is the distance between the Sichuan 1987 (SI87) and Beijing 1989 (BE89) clusters, which are genetically closely related but antigenically distinct. The difficulties with an antigenic interpretation of genetic data include the variation in the antigenic effect of amino acid substitutions because of the particular amino acid substitution, the location of the substitution, or the interaction of multiple substitutions.

Surprisingly, a single amino acid substitution, N145K (*32*), is the only cluster-difference substitution between the SI87 and BE89 and between the Beijing 1992 (BE92) and Wuhan 1995 (WU95) clusters. This is surprising because other cluster transitions are characterized by multiple cluster-difference substitutions and because, on average, a single amino acid substitution causes only 0.37 units of antigenic change. Three pieces of evidence, however, indicate that N145K has a large antigenic effect and, thus, alone can be responsible for a cluster transition. First, there are 12 pairs of strains in the dataset that only differ by N145K, and the average antigenic distance between these pairs in the antigenic map is 4.0 units (SD 1.1). In contrast, other amino acid substitutions at the same position (I145S, N145S), and the same substitution at a different position (N92K), each resulted in less than 1 unit of antigenic change. Second, we took a strain from the BE92 cluster and performed experimental site-directed mutagenesis of position 145 from N to K, and this resulted in 2.6 units of antigenic difference. Third, there were nine strains in the genetic map for which the genetic cluster did not correspond with the antigenic cluster, and N145K was responsible for the difference. These nine strains were interdigitated between the BE92 and WU95 clusters: Five strains from the BE92 antigenic cluster were genetically WU95-like but lacked the N145K substitution [seen as pink triangles in the green WU95 genetic cluster (Fig. 3)], and vice versa, four strains from the WU95 antigenic cluster were genetically BE92-like but had the N145K substitution [shown as green circles in the pink BE92 genetic cluster (Fig. 3)]. To exclude the possibility of laboratory errors, we resequenced and regenerated the HI data for seven of these interdigitated strains and obtained the same results. These three pieces of evidence indicate that a single amino acid substitution, in this case N145K, can cause sufficient antigenic change to be responsible for a cluster transition. Thus, although there is a remarkable correspondence between the genetic and antigenic evolution, there are exceptions that have epidemiological significance of sufficient magnitude that they require an update of the vaccine strain.

Gradual genetic evolution, but punctuated antigenic evolution. A season-by-season analysis of the clusters in the antigenic map shows that in some seasons strains were isolated from more than one antigenic cluster (Fig. 4A). On average, clusters remained dominant for 3.3 years (SD 1.9), with two clusters being dominant for only one season and one for eight seasons. In this dataset, we see strains appear in a cluster up to 2 years before, and 2 years after, the period in which that cluster is the dominant cluster.

The corresponding season-by-season analysis of ML tree distances (Fig. 4B) shows that the rate of genetic change is relatively continuous compared with the rate of antigenic change (Fig. 4A), which is more punctuated. Because this relatively continuous rate of change may in part be due to silent nucleotide substitutions, we repeated the analysis using the number of amino acid substitutions between strains instead of the ML tree distance (Fig. 4C) and found gaps between some clusters, but still a gradual accumulation of mutations, which is not reflected in the corresponding antigenic figure. This finding suggests that some of these amino acid substitutions have little antigenic effect or an effect spreading the cluster sideways in relation to the distance from A/Bilthoven/16190/68 antigen.

The average rates of evolution are given by the slope of the best linear fit to the data in Fig. 4, A, B, and C. The average rate of antigenic drift calculated this way was 1.2 units per year, the average rate of amino acid substitutions was 3.6 per year, and the average rate of change in ML distance was 0.0060 per year. Sometimes the rate of antigenic evolution was faster than genetic evolution and sometimes vice versa, as shown by the deviations from the linear regression line in

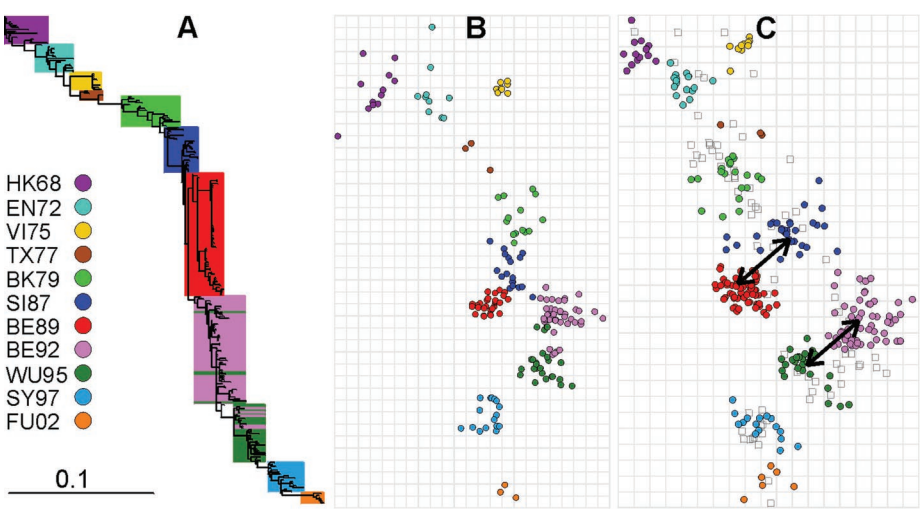

Fig. 2. Comparison of antigenic and genetic evolution of influenza A virus. (**A**) Phylogenetic tree of the HA1 nucleotide sequences, color-coded based on antigenic clusters of Fig. 1. Multiple trees were built using a reversible site-dependent nucleotide ML method (*37*). There was good consensus among trees, and the tree with ML is shown. (**B**) Genetic map of the HA1 amino acid sequences, color-coded according to the antigenic clusters of Fig. 1. The vertical and horizontal axes represent genetic distance, in this case the number of amino acid substitutions between strains; the spacing between grid lines is 2.5–amino acid substitutions. The orientation of the map was chosen to match the orientation of the antigenic map in Fig. 1. (**C**) The same antigenic map of influenza A virus strains as shown in Fig. 1, except for a rigid-body rotation and translation of the pre-TX77 clusters (fig. S2) to match the genetic map and except that virus strains are represented by colored circles and antisera by open squares. Arrows indicate the two cluster transitions for which the amino acid substitution N145K is the only cluster-difference substitution (Table 1, fig. S1).

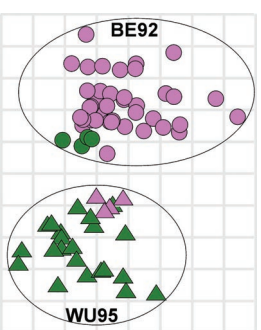

Fig. 3. Detail of the genetic map (Fig. 2B) showing the BE92 and WU95 clusters and how a single amino acid substitution can determine the antigenic cluster. Pink and green symbols represent strains from the BE92 and WU95 antigenic clusters, respectively. Ovals are drawn around the BE92 (circles) and WU95 (triangles) genetic clusters. Green symbols have a lysine (K) at position 145, whereas pink symbols have an asparagine (N) at 145. This single N145K substitution can cause an antigenic cluster change and warrant an update of the vaccine. Two pink triangles are coincident thus only four of the five can be seen. Grid and axes are the same as for Fig. 2B.

Fig. 4D, again, this indicates a remarkable correspondence, with significant exceptions.

The observed pattern of clustered antigenic drift with similar antigenic distances between consecutive cluster centroids is similar to that observed by Gog and Grenfell in a theoretical model in which strain dynamics were governed by a combination of epidemiology and cross-reactive immunity based on antigenic distance (*33*). This similarity is phenotypic evidence that escape from immunity in the human population plays a major role in determining influenza strain dynamics. Furthermore, there is a selective advantage for clusters that move away linearly from previous clusters as they most effectively escape existing population-level immunity, and this is a plausible explanation for the somewhat linear antigenic evolution in regions of the antigenic map (Fig. 1). The observed deviations from a linear path, as well as the rate of the antigenic evolution, might be determined by tradeoffs between intrinsic viral fitness and extrinsic fitness determined by population-level immunity, possibly in concert with stochastic seeding processes (*34*), short-lived broad immunity (*13*), and the phylodynamics of the virus (*35*).

Genetic analyses of Darwinian selection on influenza HA have focused on the gene level, with more recent refinements to the codon level (*10*). The quantification of antigenic data described here, which allows the estimation of the antigenic effect of individual amino acid substitutions, provides the opportunity for analyses which integrate selection at the phenotypic level with genetic change at the level of individual amino acid substitutions.

In summary, we have presented a quantification and visualization of the antigenic evolution of influenza A (H3N2) virus from 1968 to 2003 and have tested the accuracy of the method using blind prediction. We show that antigenic evolution is clustered and mostly two-dimensional and reveal a higher rate of antigenic evolution between clusters than within clusters, a remarkable correspondence between antigenic and genetic evolution, but with important exceptions of epidemiological significance, and punctuated antigenic evolution compared with more continuous genetic evolution. The data used for this study were collected as part of routine influenza surveillance, and although there are significant biases in such data, these biases do not have a significant effect on the results (*9*). This is the most detailed characterization of a real antigenic shape space to date.

From a public health perspective, these methods increase the value of surveillance data and facilitate vaccine strain selection by allowing a finer-grain interpretation of antigenic data, a way to interpret complex data in a simple visual format, and a further integration of antigenic and genetic data. In addition, antigenic maps, in conjunction with strain prevalence data, could be used to quantify the extent to which emerging strains escape immunity in the human population. This would allow the immune-escape component of viral fitness to be compared among multiple cocirculating strains and, if immune-escape is a dominant aspect of total fitness, to be a predictor of which strains would be more likely to seed a new epidemic. It might also be possible to increase the efficacy of repeated vaccination by accounting quantitatively for the antigenic distances among vaccine and circulating strains (*23*).

We have used human influenza A (H3N2) virus to develop and validate analyses of antigenic properties from binding assay data. We have applied the same methods to the characterization of human H1N1, swine H3N2, and equine H3N8 influenza A viruses, as well as human influenza B virus. There are no assumptions that limit the use of these methods to influenza virus and the HI assay, and we have also applied the methods to the recognition of epitopes by cytotoxic T lymphocytes. We expect these methods will apply to other binding assays such as virus neutralization, complement fixation, and ELISA (*36*) and that they will be useful for a wide variety of antigenically variable pathogens including human immunodeficiency virus and hepatitis C virus. In general, these methods facilitate the analyses of phenotypes similarly to the way phylogenetic algorithms facilitate analyses of genotypes. Such quantitative analyses have potentially wide-ranging implications for strain surveillance and vaccine strain selection, and for applied and basic research involving antigenically variable pathogens.

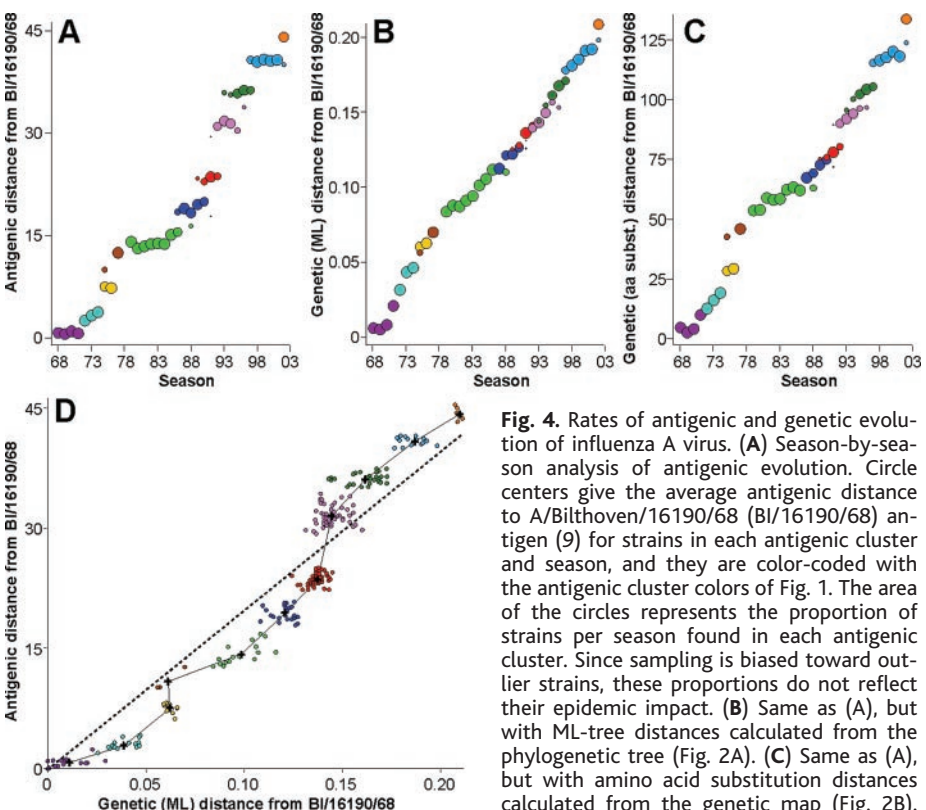

Fig. 4. Rates of antigenic and genetic evolution of influenza A virus. (**A**) Season-by-season analysis of antigenic evolution. Circle centers give the average antigenic distance to A/Bilthoven/16190/68 (BI/16190/68) antigen (*9*) for strains in each antigenic cluster and season, and they are color-coded with the antigenic cluster colors of Fig. 1. The area of the circles represents the proportion of strains per season found in each antigenic cluster. Since sampling is biased toward outlier strains, these proportions do not reflect their epidemic impact. (**B**) Same as (A), but with ML-tree distances calculated from the phylogenetic tree (Fig. 2A). (**C**) Same as (A), but with amino acid substitution distances calculated from the genetic map (Fig. 2B). (**D**) Comparison of antigenic and genetic evolution. Points are color-coded according to antigenic cluster. The solid line connects the cluster centroids, the dashed line is the best linear fit to the data with a forced zero-intercept.

References and Notes

1. G. K. Hirst, *J. Exp. Med.* **78**, 407 (1943).
2. D. D. Richman, T. Wrin, S. J. Little, C. J. Petropoulos, *Proc. Natl. Acad. Sci. U.S.A.* **100**, 4144 (2003).
3. D. H. O'Connor *et al.*, *Nature Med.* **8**, 493 (2002).
4. A. Lapedes, R. Farber, *J. Theor. Biol.* **212**, 57 (2001).
5. K. Stohr, *Lancet Infect. Dis.* **2**, 517 (2002).
6. A. W. Hampson, in *Influenza*, C. W. Potter, Ed. (Elsevier, London, 2002), pp. 49–85.
7. J. E. Salk, P. C. Suriano, *Am. J. Public Health* **39**, 345 (1949).
8. E. D. Kilbourne *et al.*, *Proc. Natl. Acad. Sci. U.S.A.* **99**, 10748 (2002).
9. Materials and methods are available as supporting material on *Science* Online. For software, see www.antigenic-cartography.org.
10. R. M. Bush, W. M. Fitch, C. A. Bender, N. J. Cox, *Mol. Biol. Evol.* **16**, 1457 (1999).
11. R. M. Bush, C. A. Bender, K. Subbarao, N. J. Cox, W. M. Fitch, *Science* **286**, 1921 (1999).
12. J. B. Plotkin, J. Dushoff, S. A. Levin, *Proc. Natl. Acad. Sci. U.S.A.* **99**, 6263 (2002).
13. N. M. Ferguson, A. P. Galvani, R. M. Bush, *Nature* **422**, 428 (2003).
14. P. H. A. Sneath, R. R. Sokal, *Numerical Taxonomy* (Freeman, San Francisco, 1973).
15. T. F. Weijers *et al.*, *J. Virol. Methods* **10**, 241 (1985).
16. D. J. Alexander *et al.*, *Avian Pathol.* **26**, 399 (1997).
17. P. A. Underwood, *J. Gen. Virol.* **62** (Pt. 1), 153 (1982).

18. A. Dekker, G. Wensvoort, C. Terpstra, *Vet. Microbiol.* **47**, 317 (1995).
19. J. M. Daly *et al.*, *J. Gen. Virol.* **77** (Pt. 4), 661 (1996).
20. A. S. Perelson, G. F. Oster, *J. Theor. Biol.* **81**, 645 (1979).
21. L. Edelstein, R. Rosen, *J. Theor. Biol.* **73**, 181 (1978).
22. D. J. Smith, S. Forrest, A. S. Perelson, in *Artificial Immune Systems and Their Applications*, D. Dasgupta, Ed. (Springer Verlag, Berlin, 1998), pp. 105–114.
23. D. J. Smith, S. Forrest, D. H. Ackley, A. S. Perelson, *Proc. Natl. Acad. Sci. U.S.A.* **96**, 14001 (1999).
24. J. Kruskal, *Psychometrika* **29**, 115 (1964).
25. R. Shepherd, *Hum. Factors* **5**, 33 (1963).
26. Newly sequenced HA1 domain accession numbers: AY660991-AY661211. Previously published HA1 domain accession numbers are in the supporting material.
27. C. A. Macken, H. Lu, J. Goodman, L. Boykin, in *Options for the Control of Influenza IV*, A. D. M. E. Osterhaus, N. Cox, A. W. Hampson, Eds. (Elsevier Science B.V., Amsterdam, 2001), pp. 103–106.
28. D. C. Wiley, I. A. Wilson, J. J. Skehel, *Nature* **289**, 373 (1981).
29. I. A. Wilson, J. J. Skehel, D. C. Wiley, *Nature* **289**, 366 (1981).
30. G. W. Both, M. J. Sleigh, N. J. Cox, A. P. Kendal, *J. Virol.* **48**, 52 (1983).
31. A. J. Hay, V. Gregory, A. R. Douglas, Y. P. Lin, *Philos. Trans. R. Soc. London B. Biol. Sci.* **356**, 1861 (2001).
32. Single-letter abbreviations for the amino acid residues are as follows: I, Ile; K, Lys; N, Asn; and S, Ser.
33. J. R. Gog, B. T. Grenfell, *Proc. Natl. Acad. Sci. U.S.A.* **99**, 17209 (2002).
34. J. R. Gog, G. F. Rimmelzwaan, A. D. Osterhaus, B. T. Grenfell, *Proc. Natl. Acad. Sci. U.S.A.* **100**, 11143 (2003).
35. B. T. Grenfell *et al.*, *Science* **303**, 327 (2004).
36. D. A. Lennette, in *Diagnostic Procedures for Viral, Rickettsial and Chlamydial Infections*, E. H. Lennette, D. A. Lennette, E. T. Lennette, Eds. (American Public Health Association, Washington, DC, 1995).
37. B. Korber *et al.*, *Science* **288**, 1789 (2000).
38. We thank R. van Beek, W. Beyer, T. Bhattacharya, R. Bush, N. Cox, B. Grenfell, J. Gog, H. Gutowitz, A. Hay, R. Hightower, T. Jones, A. Tang, the contributors to the WHO global influenza surveillance network, and the maintainers of the Influenza Sequence Database (www.flu.lanl.gov). We acknowledge the support of the Santa Fe Institute and the Dutch National Institute of Public Health and the Environment (RIVM). D.J.S. was supported by European Union grant QLRT-2001-01034. A.S.L. was supported by the U.S. Department of Energy, contract W-7405-ENG-36, under the Laboratory-Directed Research and Development program. R.A.M.F. is a fellow of the Royal Dutch Academy of Arts and Sciences.

Supporting Online Material
www.sciencemag.org/cgi/content/full/1097211/DC1
Materials and Methods
Figs. S1 to S3
Table S1
References and Notes

26 February 2004; accepted 11 June 2004
Published online 24 June 2004;
10.1126/science.1097211
Include this information when citing this paper

REPORTS

Phase-Resolved Spectroscopy of Geminga Shows Rotating Hot Spot(s)

P. A. Caraveo,[1]* A. De Luca,[1] S. Mereghetti,[1] A. Pellizzoni,[1] G. F. Bignami[2,3,1]

Isolated neutron stars are seen in x-rays through their nonthermal and/or surface thermal emissions. X-ray Multimirror Mission–Newton observations of the Geminga pulsar show a 43–electron volt spectrum from the whole neutron star surface, as well as a power-law component above 2 kiloelectron volts. In addition, we have detected a hot (170 electron volts) thermal emission from an ~60-meter-radius spot on the pulsar's surface. Such a thermal emission, only visible at selected phase intervals, may be coming from polar hot spot(s), long thought to exist as a result of heating from magnetospheric accelerated particles. It may provide the missing link between the x-ray and gamma-ray emission of the pulsar.

Photons emitted by pulsars carry the signature of their production mechanisms as well as of the geometry of their emitting regions. Although neutron star physics is reflected in their photon spectra, geometrical constraints, such as viewing angles of rotational and magnetic axes, shape their observed light curves. Phase modulation takes place as different emitting regions are brought into view during the star rotation. Geometry can also influence source spectral shapes because of different emission mechanisms in different regions.

In spite of the potential interest of phase-resolved spectroscopy, the paucity of detected x-ray photons has made it impossible to apply this method to isolated neutron stars (INS), with the exception of the Crab pulsar (*1*). The European Photon Imaging Camera (EPIC) on XMM-Newton and Chandra can now provide an adequate harvest of time-tagged photons. However, phase-resolved spectroscopy is not yet commonly used. So far, it has been applied only to the Crab pulsar with Chandra (*2*) and to 1E1207-5209 with EPIC (*3*, *4*). Although interesting, these sources represent specific and somewhat extreme cases among x-ray–emitting neutron stars. The Geminga pulsar, on the other hand, is often considered as archetypal (*5*) for middle-aged (350,000 years old) neutron stars, which emit x-rays mostly, but not solely, owing to their surface thermal emission. INS surface temperatures frequently yield radiation in the x-ray domain (*6*), but keV photons can also be produced by energetic electrons in their strong magnetic fields. Geminga has the interesting characteristic of showing both thermal (*7*) and nonthermal processes to be at work in the sub-keV to several keV range (*8*, *9*). With a photon number more than doubling all previous statistics, and with a wider (0.15 to 8 keV) spectral range, EPIC now offers the chance of a meaningful phase-resolved spectroscopy for Geminga.

XMM-Newton performed a 100-ksec exposure on 4 April 2002 with its three EPIC cameras. The two metal-oxide semiconductor (MOS) cameras (*10*) operated in "full frame" mode, while the positive-negative (pn) camera (*11*) operated in "small window" mode, ideal for accurate timing of source photons. After removing intervals with high particle background and correcting for dead time, we obtain a net exposure of 55.0 ksec for the pn camera and of 76.9 and 77.4 ksec for MOS1 and MOS2, respectively. The EPIC observation yielded a total of 76,850 photons in the energy range $0.15 < E < 8$ keV, the majority of which (52,850 photons) are due to the pn detector. The MOS images have unveiled two tails of diffuse emission that are trailing Geminga and are well aligned with the source proper motion (*12*). Here, we present the analysis of the pn data, which were processed with the XMM-Newton Science Analysis Software (SAS version 5.4.1).

First, we have fitted the time-averaged, total source data (Fig. 1), using a combination of a black body and a power law. In view of the unsatisfactory result, we added a third component, both in the form of a black body and of a power law. The resulting χ^2 improved significantly, which suggests that Geminga's spectrum indeed requires a three-component model.

[1]Istituto di Astrofisica Spaziale e Fisica Cosmica, Consiglio Nazionale delle Ricerche, Via Bassini, 15-20133 Milano, Italy. [2]Centre d'Étude Spatiale des Rayonnements, Centre National de la Recherche Scientifique, Université Paul Sabatier, 9 Avenue du Colonel Roche, Toulouse, France. [3]Università di Pavia, Dipartimento Fisica Teorica e Nucleare, Via Ugo Bassi, 6 Pavia, Italy.

*To whom correspondence should be addressed. E-mail: pat@mi.iasf.cnr.it